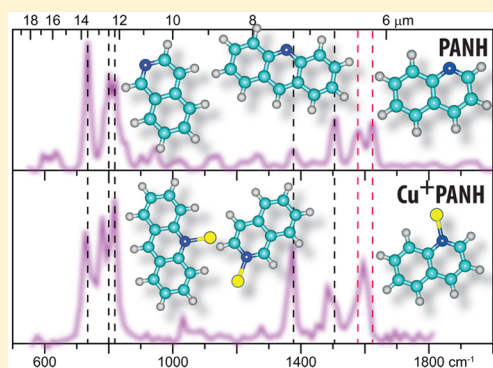


# The Influence of Metal Ion Binding on the IR Spectra of Nitrogen-Containing PAHs

Juehan Gao,<sup>†</sup> Jordy Bouwman,<sup>†</sup> Giel Berden,<sup>†</sup> and Jos Oomens<sup>\*,†,‡</sup><sup>†</sup>Radboud University, FELIX Laboratory, Institute for Molecules and Materials, Toernooiveld 7c, 6525ED Nijmegen, The Netherlands<sup>‡</sup>Van't Hoff Institute for Molecular Sciences, University of Amsterdam, Science Park 904, 1098XH Amsterdam, The Netherlands

## Supporting Information

**ABSTRACT:** Astronomical IR emission spectra form the basis for the now widely accepted abundant presence of polycyclic aromatic hydrocarbons (PAHs) in inter- and circumstellar environments. A small but consistent frequency mismatch is found between the astronomically observed emission band near 6.2  $\mu\text{m}$  and typical CC-stretching vibrations of PAHs measured in laboratory spectra near 6.3–6.4  $\mu\text{m}$ . The shift of the band has been tentatively attributed to a variety of effects, among which the inclusion of heteroatoms, in particular nitrogen, in the PAH skeleton (PANH) as well as to metal ion binding to the PAH molecule. Here we experimentally investigate the combined effect of nitrogen-inclusion and metal ion binding on the IR spectra. In particular, infrared multiple-photon dissociation (IRMPD) spectra are recorded for coordination complexes of  $\text{Cu}^+$  with one or two quinoline, isoquinoline, and acridine ligands; complexes of the form  $\text{Cu}^+(\text{PANH})$  (MeCN), where the MeCN (acetonitrile) ligand acts as a relatively weakly bound “messenger” are also recorded to qualitatively verify that potential frequency shifts induced by IRMPD are minimal. The experimental IR spectra document the accuracy of IR spectral predictions by density functional theory calculations performed at the B3LYP/6-311+G(2df,2p) level and confirm that a  $\sigma$ -bond is formed between the copper ion and the exoskeletal N atom. The experimental spectra suggest that the CNC stretching mode undergoes a small red shift of up to 20  $\text{cm}^{-1}$ , with respect to the band position in the uncomplexed PANH molecule, away from the 6.2  $\mu\text{m}$  interstellar position.



## 1. INTRODUCTION

Polycyclic aromatic Hydrocarbons (PAHs) molecules are hypothesized to be abundant species in the Interstellar Medium (ISM), based mainly on the ubiquitous mid infrared (mid-IR) emission bands that are centered at wavelengths near 3.3, 6.2, 7.7, 8.8, 11.3, and 12.7  $\mu\text{m}$ .<sup>1–4</sup> These emission bands arise when PAHs are excited by UV radiation and subsequently undergo internal conversion and radiative vibrational relaxation. Variations in relative intensity, peak position, and peak profile are extensively used as a probe of the physical properties of the PAH families present in regions of the ISM.<sup>2,4–6</sup>

Experimental studies on the IR spectra of PAH cations revealed that the CC-stretching feature measured in laboratory spectra is generally red-shifted compared to the band observed in the ISM near 6.2  $\mu\text{m}$ .<sup>7–10</sup> Since nitrogen is the fourth most abundant element, it was hypothesized that nitrogen containing PAHs (PANHs) may also be present in the ISM.<sup>6,9,11</sup> The effects of N atom substitution on the frequency of the dominant CC stretching modes of PANH cations were illustrated in a number of theoretical and experimental spectroscopic studies,<sup>6,9,11–14</sup> revealing that the band indeed shifts in the direction of the 6.2  $\mu\text{m}$  interstellar emission band.

Another mechanism that has been hypothesized to be responsible for a small but significant blue shift of the CC

stretch modes is the attachment of metal cations to the PAH molecule. Silicon as well as various metals including Fe, Na, Mg, Al, and Cu exist in varying abundances in the ISM.<sup>15–19</sup> These metals often do not occur as isolated atoms or ions, but may be sequestered by molecules and dust particles and, as a result, the elemental metals are depleted.<sup>20–34</sup> Metal-PAH clusters are thought to be formed in dense molecular clouds and consequently, their astrophysical relevance has received considerable attention.<sup>26,35–47</sup>

Experimental laboratory data on metal-ion PAH complexes of interest focus mainly on thermochemical properties including, in particular, binding energies and reaction kinetics.<sup>40,42,43,48,49</sup> On the other hand, IR spectroscopic data reported for metal-ion PAH complexes largely concern theoretically predicted spectra, typically computed using density functional theory (DFT)<sup>50–54</sup> as well as other computational methods.<sup>55,56</sup> However, spectral shifts upon metal ion complexation may be subtle and the performance of the computational method of choice may not be precisely known, especially for complexes involving transition metal ions.

Received: May 19, 2016

Revised: September 19, 2016

Published: September 20, 2016

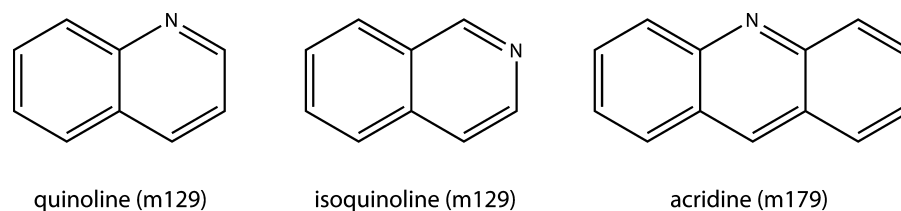


Figure 1. PANH ligands studied in this work with their molecular weight given in brackets.

Experimental gas-phase IR spectra can verify the reliability of computational values. As often the case, more constraints apply to experimental investigations than to computational ones, and only relatively few experimental gas-phase IR spectra of metal–ion PAH complexes have been reported to date. Using a combination of tandem mass spectrometry and laser spectroscopy,<sup>57–59</sup> small mass-isolated  $\text{Fe}^+$ PAH complexes formed via laser ablation of an iron target have been spectroscopically investigated revealing their  $\pi$ -bound nature.<sup>45,46</sup> IR spectra for  $\text{Ag}^+$ –naphthalene complexes formed by electrospray ionization (ESI) have been obtained using IR messenger spectroscopy of Ne-tagged complex ions, establishing their structures also as  $\pi$ -bound complexes.<sup>60</sup> In general, these studies showed that the IR absorption bands in the 6.2  $\mu\text{m}$  region are blue-shifted as compared to the uncomplexed PAH.

Unlike for PAHs, the effects of metal ion binding on the characteristic vibrational frequencies of PANHs, i.e., the combined effect of nitrogen inclusion and metal ion attachment, have not been subject of detailed experimental study. As far as we are aware, the only IR spectroscopic study of a metal ion clustering with a cyclic nitrogen containing hydrocarbon is reported by Dopfer and co-workers,<sup>47</sup> who studied the structure of the  $\text{Ag}^+(\text{Pyridine})_2$  complex by infrared multiple-photon dissociation (IRMPD) spectroscopy. The  $\text{Ag}^+$  ion was reported to bind to the lone pair electrons of the pyridine, forming a planar  $\sigma$ -bound complex. Here we report on IR spectra in the 5.5–17  $\mu\text{m}$  range of gaseous complexes of  $\text{Cu}^+$  with a selection of small PANH molecules (quinoline, isoquinoline, and acridine; see Figure 1). Experimental spectra are compared with computed spectra to address in particular (1), whether there is an observable effect on the spectra of the PANH, especially in the region near 6.2  $\mu\text{m}$ , and (2) whether DFT calculated spectra—at the B3LYP level—reproduce these changes.

Relevant data available for these  $\text{Cu}^+$ PANH systems include gas-phase molecular structure information derived from threshold collision induced dissociation (TCID) in combination with theoretical modeling.<sup>61,62</sup> In these studies, the binding energies for a number of complexes of  $\text{Cu}^+$  with small N-containing heterocyclic compounds were determined. Moreover, a  $\sigma$ -bound structure where the  $\text{Cu}^+$  ion coordinates to the nitrogen lone-pair was clearly established in these experiments.

## 2. EXPERIMENTAL AND THEORETICAL METHODS

**2.1. Experiment.** IRMPD spectra of complexes of  $\text{Cu}^+$  with PANH molecules have been measured over the 5.5–17  $\mu\text{m}$  wavelength range in a Fourier-transform ion cyclotron resonance mass spectrometer (FTICR-MS)<sup>63</sup> coupled to one of the beam ports of the Free Electron Laser for Infrared eXperiments (FELIX).<sup>58,64</sup> The combination of the mass spectrometer and the free electron laser has been used in a variety of studies and has been described in detail elsewhere.<sup>58,65</sup>

Complex stoichiometries studied are  $\text{Cu}^+(\text{PANH})_1$ ,  $\text{Cu}^+(\text{PANH})\text{MeCN}$ , and  $\text{Cu}^+(\text{PANH})_2$ , where MeCN refers to acetonitrile. The PANH (quinoline 97%, isoquinoline 97%, acridine 97%) samples were purchased from Tokyo Chemical Industry (TCI) and used without further purification. The complexes were generated through ESI of solutions containing 200  $\mu\text{M}$   $\text{CuCl}$  and 250  $\mu\text{M}$  PANH in neat MeCN. The ionic complexes are accumulated in a linear hexapole ion trap prior to being injected into the ICR cell through an octopole RF ion guide. Copper has two isotopes occurring in significant natural abundance (<sup>63</sup>Cu at 69.2% and <sup>65</sup>Cu at 30.8%) so that complexes are detected as double peaks in the mass spectra. The  $\text{Cu}^+(\text{PANH})_2$  and  $\text{Cu}^+(\text{PANH})\text{MeCN}$  complexes are generated directly from the ESI source. The generation of the monomeric  $\text{Cu}^+(\text{PANH})_1$  is more challenging and requires a different approach: the  $\text{Cu}^+(\text{quinoline})\text{MeCN}$  and  $\text{Cu}^+(\text{quinoline})_2$  precursor ions are irradiated for 5 s with a 35-W cw  $\text{CO}_2$  laser in the high vacuum of the ICR cell, after which the monoligated complex thus formed is mass-isolated. For  $\text{Cu}^+(\text{isoquinoline})_1$  and  $\text{Cu}^+(\text{acridine})_1$ , 2 s of  $\text{CO}_2$  laser irradiation is sufficient. Even if the produced ions were internally hot, the time scale of the experiments is such that the ions have ample time to cool radiatively before being probed by IRMPD spectroscopy.<sup>66</sup>

Mass isolation is achieved by means of a stored-waveform inverse Fourier-transform (SWIFT) excitation pulse in the Penning trap of the FTICR-MS.<sup>63</sup> Subsequently, the mass filtered clusters are irradiated by the (attenuated) IR radiation of the free electron laser. Monitoring the IR induced fragment ion yield as a function of wavelength allows one to reconstruct an IR spectrum of the  $\text{Cu}^+$ /PANH ion. IR spectra are recorded with a pulse energy of about 35 mJ per FEL macropulse (5  $\mu\text{s}$ ), and the measured IRMPD yield is normalized to the laser pulse energy assuming a linear dependence. The fwhm spectral bandwidth of the FEL was set to about 0.5% of the central wavelength, which amounts to 5  $\text{cm}^{-1}$  at 10  $\mu\text{m}$  and the step size during the wavelength scans was around 5  $\text{cm}^{-1}$ . The laser wavelength was calibrated using a grating spectrometer with an array detector; the dispersion is 0.020  $\mu\text{m}$  per array element (2  $\text{cm}^{-1}$  at 10  $\mu\text{m}$ ).

**2.2. Computational Aspects.** Quantum-chemical computations have been performed at the DFT level using the Gaussian09 Rev. D.01 program package. The geometries of the  $\text{Cu}^+(\text{PANH})$  complexes are optimized and vibrational frequencies are calculated using the B3LYP functional and 6-311+G(2df,2p) basis set. The  $\text{Cu}^+$  ion has a  $3d^{10}$  ground state, and only singlet electronic states were considered for the complexes. Unrestricted calculations on a few of the systems under study returned  $S^2$  values equal to 0.00 indicating that spin contamination is not a problem for these complexes. Electronic energies were corrected for zero-point energy (ZPE) and relative Gibbs free energies were determined at 298 K. Counterpoise corrections have been explored to correct

computed energies for possible basis set superposition errors (BSSE) for all  $\text{Cu}^+(\text{PANH})$  complexes. Orbital populations, partial charges and natural bond orbitals have been analyzed using Natural Population Analysis (NPA) and Natural Bond Orbitals (NBO, version 3.1), all as implemented in Gaussian09. The computed harmonic vibrational frequencies are scaled by a factor of 0.965 to empirically account for unknown anharmonicities, close to values recommended by the NIST CCCBDB online database<sup>67</sup> (0.967) and by Radom and co-workers (0.9686).<sup>68</sup> Computed spectra are convoluted with a  $15\text{ cm}^{-1}$  full width at a half-maximum (fwhm) Gaussian profile to facilitate comparison with the measured spectra.

### 3. RESULTS

Prior to presenting the IR spectral data, we briefly discuss a few features of the electronic and geometric structures of the  $\text{Cu}^+$ /PANH complexes that result from the DFT calculations.

**3.1. Computed Structure Properties.** In all  $\text{Cu}^+$ /PANH complexes studied, the  $\text{Cu}^+$  ion is  $\sigma$ -coordinated to the nitrogen atom of the PANH. Optimizations starting from a  $\pi$ -complex geometry relaxed to the N-bound  $\sigma$ -complex structure. In dimeric  $\text{Cu}^+$ /PANH complexes, both ligands arrange at  $180^\circ$  around the  $\text{Cu}^+$  center. The electron configuration of  $\text{Cu}^+$  ( $3d^{10} 4s^0$ ) is known to give rise to  $sd$ -hybridization due to the energetic proximity of the  $3d$  and  $4s$  orbitals.<sup>61</sup> This results in two hybrid atomic orbitals, of which one is unoccupied having lobes at  $180^\circ$ .  $N$ -donor atoms of the ligands can donate electron density into this empty  $sd$  hybrid orbital to form a linear arrangement of the two ligands around the metal center. The NPA calculation indicates that this  $sd$ -hybridization results in an electron configuration of  $3d^{9.80} 4s^{0.50} 4p^{0.10}$  for  $\text{Cu}^+(\text{acridine})_2$ ,  $3d^{9.78} 4s^{0.50} 4p^{0.06}$  for  $\text{Cu}^+(\text{isoquinoline})_2$ , and  $3d^{9.79} 4s^{0.49} 4p^{0.07}$  for  $\text{Cu}^+(\text{quinoline})_2$ . These values are similar to those found for other dimeric  $N$ -donor complexes of  $\text{Cu}^+$ .<sup>61,62,69</sup>

Partial charges on the metal ion assigned by the NPA analysis for each of the complexes are listed in Table 1. The low partial

**Table 1. Partial Charges on the Cu Atom in the Various  $\text{Cu}^+$ /PANH Complexes As Computed by the Natural Population Analysis**

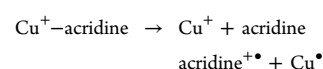
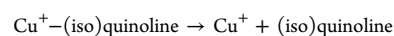
ligand(s)	$\text{Cu}^+$ partial charge
2 acridine	+0.594
acridine + MeCN	+0.667
acridine	+0.804
2 quinoline	+0.640
quinoline + MeCN	+0.685
quinoline	+0.832
2 isoquinoline	+0.662
isoquinoline + MeCN	+0.698
isoquinoline	+0.844

charge found on the  $\text{Cu}^+$  ion, ranging between approximately +0.6  $e$  for bis-ligated complexes and approximately +0.8  $e$  for the monoligated  $\text{Cu}^+(\text{PANH})$  complexes suggests that a substantial charge transfer to the metal occurs. As expected, having a lower ionization potential (IP), the acridine ligand (7.8 eV)<sup>70</sup> donates more charge to the Cu ion than the quinoline (8.6 eV) and isoquinoline (8.5 eV) ligands, having a higher IP. Note that the IP of Cu (7.72 eV) is close to that of acridine.

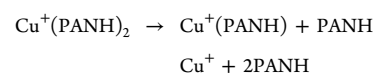
NBO analyses were performed on the  $\text{Cu}^+(\text{PANH})_1$  systems. The main orbital interaction is in all cases observed for the

nitrogen lone pair orbital donating into the Cu  $4s$ -orbital, leading to a stabilization on the order of 180 kJ/mol. Backdonation is relatively small, with the largest contribution stemming from interaction between one of the Cu  $3d$  orbitals and the CN antibonding virtual orbital contributing about 6 kJ/mol.

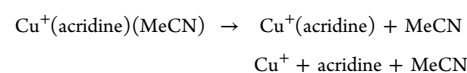
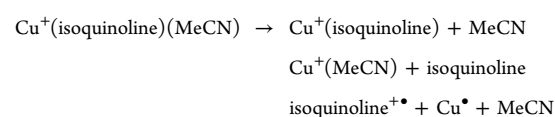
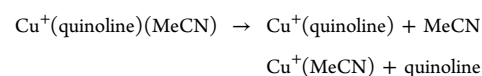
**3.2. IR Spectra.** The mid-IR spectra of the  $\text{Cu}^+$ -complexed PANHs are recorded by IRMPD spectroscopy. The  $\text{Cu}^+(\text{PANH})_1$  species dissociate by loss of the neutral ligand, but for  $\text{Cu}^+(\text{acridine})_1$  the acridine radical cation is also observed, likely on account of the lower IP of acridine as compared to those of quinoline and isoquinoline:<sup>70</sup>



The  $\text{Cu}^+(\text{PANH})_2$  clusters expel one or two ligands upon resonant irradiation, where the latter channel is likely a secondary process, which was not observed for  $\text{Cu}^+(\text{isoquinoline})_2$ :



Observed dissociation channels for the  $\text{Cu}^+(\text{PANH})$  (MeCN) complexes were:



The accompanying neutral losses are inferred in the above equations.

Dissociation energies ( $D_e$ ) of  $\text{Cu}^+\text{PANH}$  complexes have been computed and are summarized in Table 2. The binding of the first ligand to  $\text{Cu}^+$  is obviously the strongest. This manifests itself in the IR experiments by a weak IRMPD signal for the monomeric complexes and inherent low signal-to-noise spectral data. More facile dissociation of the  $\text{Cu}^+(\text{PANH})_2$  and  $\text{Cu}^+(\text{PANH})$  (MeCN) complexes results in spectra with

**Table 2. Computed Adiabatic Dissociation Energies (given as  $D_e$ ,  $D_0$ , and  $\Delta G^0$ ) of the Various  $\text{Cu}^+$ /PANH Complexes Studied in This Work (in kJ/mol)**

ligand(s) on $\text{Cu}^+$	neutral loss	$D_e$	$D_e^{a\ddagger}$	$D_0$	$\Delta G^0$
2 acridine	acridine	243	239	238	182
acridine + MeCN	MeCN	214	211	213	166
acridine	acridine	319	316	313	277
2 quinoline	quinoline	245	242	242	188
quinoline + MeCN	MeCN	222	219	222	174
quinoline	quinoline	301	299	297	261
2 isoquinoline	isoquinoline	251	248	249	198
isoquinoline + MeCN	MeCN	224	221	223	177
isoquinoline	isoquinoline	304	302	300	263

<sup>a</sup>Corrected for BSSE.

significantly better S/N ratios. Recording IRMPD spectra for species with higher and lower dissociation thresholds also allows us to qualitatively assess the effect of multiple photon excitation on band positions, in particular whether significant red-shifting occurs, which could compromise frequency comparisons with absorption spectra for neutral, uncomplexed PANHs. For the  $\text{Cu}^+(\text{PANH})_2$  complexes, energies listed are for the eclipsed geometry conformers and not for the planar conformers, because the Gibbs free energy of the eclipsed geometry is slightly lower in energy (on the order of 1 kJ/mol), as was also found for other dimeric complexes of  $\text{Cu}^+$  and N-containing ligands.<sup>61</sup> Differences in vibrational frequencies between the two structures are negligible.

Figures 2–4 show the experimental spectra (in black) of the studied complexes in the 600–1800  $\text{cm}^{-1}$  range. Experimental spectra of neutral quinoline, neutral isoquinoline, and neutral acridine are taken from the NIST Chemistry WebBook<sup>71</sup> and shown for comparison. Also shown are the lowest energy molecular structures and IR spectra (red) obtained from the quantum-chemical computations. The lowest energy structures for all complexes studied here are those where  $\text{Cu}^+$  forms a  $\sigma$ -bond to the lone-pair electrons on the nitrogen atom of the ligand. Vibrational bands in the spectra of the  $\text{Cu}^+(\text{PANH})$  (MeCN) complexes are well resolved and representative for the  $\text{Cu}^+(\text{PANH})$  and  $\text{Cu}^+(\text{PANH})_2$  complexes; we shall therefore mainly focus on these spectra in the discussion below. Band positions and assignments for bands with computed intensities greater than 5  $\text{km/mol}$  are summarized in Tables 3–5 for the  $\text{Cu}^+(\text{PANH})$  (MeCN) complexes. Tabulated experimental and computed band positions for the  $\text{Cu}^+(\text{PANH})$  and  $\text{Cu}^+(\text{PANH})_2$  complexes, as well as for the neutral PANH molecules are presented in Tables S1–S9 in the Supporting Information.

**3.2.1. IR Spectra of Complexes Containing  $\text{Cu}^+$  and Quinoline.** Figure 2 reproduces the experimental and theoretical IR spectra of neutral quinoline, taken from the NIST Chemistry WebBook,<sup>72</sup> and the  $\text{Cu}^+$ /quinoline complexes  $\text{Cu}^+(\text{quinoline})$ ,  $\text{Cu}^+(\text{quinoline})$  (MeCN), and  $\text{Cu}^+(\text{quinoline})_2$ . In general, a reasonable agreement is found between experimental and calculated spectra. Band positions and intensities in experimental and theoretical spectra of  $\text{Cu}^+(\text{quinoline})$  (MeCN) are summarized in Table 3 and further discussed below. Band positions for the other complexes are generally very similar to those for  $\text{Cu}^+(\text{quinoline})$  (MeCN); we discuss them only where significant deviations are observed.

The experimental spectrum of  $\text{Cu}^+(\text{quinoline})$  (MeCN) reveals a major feature between 780 and 820  $\text{cm}^{-1}$  attributed a CH out-of-plane (oop) bending mode and an oop ring deformation mode, which are just barely resolved. The weak bands that are observed just above the noise level near 1100  $\text{cm}^{-1}$  are attributed to CH in-plane (ip) bending and ip ring-deformation modes. The band measured at 1293  $\text{cm}^{-1}$  comprises features with mixed C–N–C asymmetric stretch, CC stretch, CH ip bending, and ip ring deformation character. This band is slightly red-shifted as compared to the corresponding band in bare quinoline. The experimental band around 1364  $\text{cm}^{-1}$  that is relatively strong and that is also observed in the other bis-coordinated complexes, deviates significantly from the computed normal modes at 1344 and 1386  $\text{cm}^{-1}$ , which comprise CC stretching, CH ip bending, and ip ring deformation character. The degenerate  $\text{CH}_3$  bending vibration in the acetonitrile ligand is computed at 1409  $\text{cm}^{-1}$

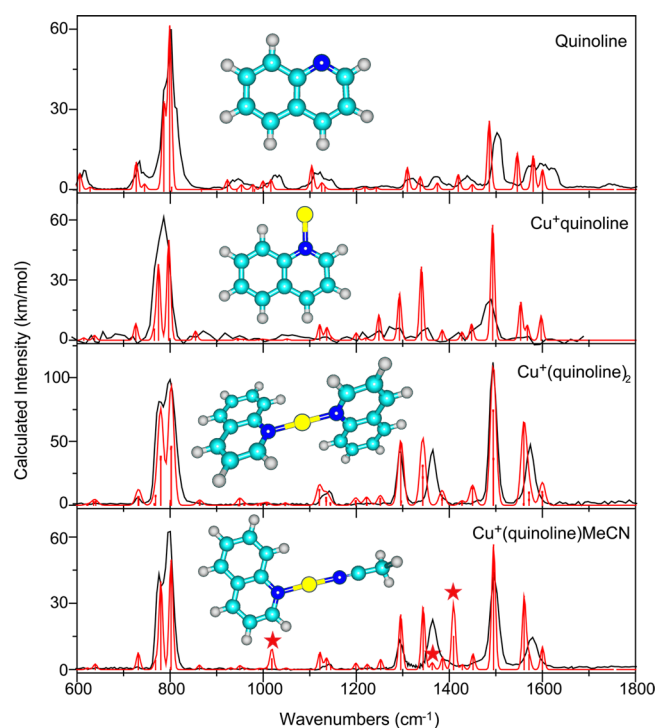


**Figure 2.** Experimental gas-phase absorption spectrum of quinoline (from the NIST webbook) and IRMPD spectra of  $\text{Cu}^+$ /quinoline complexes between 600 and 1800  $\text{cm}^{-1}$  (black) compared to computed spectra (red). Stars in the lower panel indicate vibrational bands due to the acetonitrile ligand. The units of  $\text{km mol}^{-1}$  refer to the stick spectra only.

for  $\text{Cu}^+(\text{quinoline})$  (MeCN), as indicated by the red star in Figure 2, but is not observed in the experimental spectrum, which appears to be typical for the  $\text{Cu}^+(\text{PANH})$  (MeCN) complexes studied here (*vide infra*). The intense band found near 1496  $\text{cm}^{-1}$  can be assigned to a mode with mainly CNC and CC stretching character mixed with CH ip bending and ip ring deformation character. The character of the bands predicted at 1561, 1571, and 1600  $\text{cm}^{-1}$  is best described as C–N–C asymmetric stretching, mixed with CH in plane bending, CC stretching and ip ring deformation. These bands likely correspond to the feature observed at 1579  $\text{cm}^{-1}$ .

We finally note that while the frequency predictions for the  $\text{Cu}^+(\text{quinoline})$  complex are fairly accurate, the relative intensities show a severe mismatch between experiment and theory, unlike the dimeric  $\text{Cu}^+(\text{quinoline})$  (MeCN) and  $\text{Cu}^+(\text{quinoline})_2$  complexes. Similar observations are made for the complexes with isoquinoline and acridine. We suspect that this is due to the higher binding energies of the monomeric complexes, introducing stronger deviations from linearity, manifesting itself particularly toward higher wavenumbers, where the pulse energy of the FEL gradually declines. Moreover, the modes in the high wavenumber range typically have higher anharmonicities than the oop bending modes below 1000  $\text{cm}^{-1}$ , leading to further impairing of efficient multiple photon excitation.<sup>73</sup> Somewhat similar effects were observed for experimental IRMPD spectra of complexes of  $\text{Fe}^+$  and coronene.<sup>46</sup>

**3.2.2. IR Spectra of  $\text{Cu}^+$ /Isoquinoline Complexes.** The experimental IR spectra of the three complexes including  $\text{Cu}^+$  and isoquinoline as well as the spectrum of neutral isoquinoline<sup>72</sup> compared with their calculated counterparts are shown in

**Table 3. Overview of observed and computed IR absorption band positions and intensities of Cu<sup>+</sup>(quinoline) (MeCN)**

exp. freq <sup>a</sup>	calc. freq <sup>a</sup>	dev <sup>b</sup>	int <sup>c,d</sup>	description <sup>e</sup>
732	732	0	7	CH oop bend/oop ring deform
776	780	-4	40	CH oop bend/oop ring deform
800	802	-2	49	CH oop bend/oop ring deform
	1122		8	CH ip bend/rings ip deform/CNC-Cu & CC stretch
	1136		5	CH ip bend
1293	1296	-3	25	CNC stretch/CC stretch/CH ip bend/ip ring deform
1364	1344	20	28	CC stretch/CNC stretch/CH ip bend/ip ring deform
	1386		6	CH ip bend/ip ring deform/CNC-Cu stretch/CC stretch
	1409		15	CH <sub>3</sub> degenerate bending (or CH <sub>3</sub> scissoring) of MeCN
	1409		15	CH <sub>3</sub> degenerate bending (or CH <sub>3</sub> scissoring) of MeCN
	1451		7	CH ip bend/ip ring deform/CC&CNC-Cu stretch
1496	1495	1	56	CC&CNC stretch/CH ip bend/ip ring deform/
	1561		33	CH ip bend/CC&CNC-Cu stretch/ip ring deform
1579	1571	8	7	CH ip bend/CC&CNC stretch/ip ring deform
	1600		10	CH ip bend/CC&CNC stretch/ip ring deform

RMS deviation 8.4

<sup>a</sup>In cm<sup>-1</sup>. A scaling factor of 0.965 has been applied. <sup>b</sup>exp - calc. <sup>c</sup>In km/mol. <sup>d</sup>Only bands with intensities >5 km/mol are listed. <sup>e</sup>ip = in plane; oop = out of plane.

**Figure 3.** The positions of the strongest computed and measured absorption features for Cu<sup>+</sup>(isoquinoline) (MeCN) are summarized in Table 4, while data for the other complexes containing isoquinoline are listed in Supporting Tables S4–S6.

Five main bands are observed in the IRMPD spectrum of Cu<sup>+</sup>(isoquinoline) (MeCN). The bands measured at 742 and 821 cm<sup>-1</sup> are due to CH oop bending and are well reproduced by theory. The band at 1041 cm<sup>-1</sup> corresponds to a mode involving Cu<sup>+</sup>-N and CNC symmetric stretching and is calculated at 1035 cm<sup>-1</sup>. Two weak bands observed around 1170 and 1260 cm<sup>-1</sup> are blue-shifted by 7 and 13 cm<sup>-1</sup>, respectively, compared with their computed positions; they correspond to a CH ip bending and ip ring deformation. The band measured at 1374 cm<sup>-1</sup> is stronger than the computed bands at 1360 and 1376 cm<sup>-1</sup>, having CC and CNC stretch, CH ip bend, and ip ring deformation character. For the corresponding bands in the other Cu<sup>+</sup>/isoquinoline complexes, computed and observed relative intensities are in better agreement. The MeCN degenerate CH<sub>3</sub> bending mode is computed at 1409 cm<sup>-1</sup> and is probably not observed in the IRMPD spectrum (see red star in Figure 3), although it may be comprised within the somewhat broader bands observed around this frequency. The weak and broad feature measured around 1440 cm<sup>-1</sup> corresponds to the CH ip bending and ip ring deformation modes predicted around this frequency. Finally, two bands calculated at 1583 and 1604 cm<sup>-1</sup> exhibiting Cu<sup>+</sup>-N stretching, CNC symmetric stretching, CC stretching, CH ip bending, and ip ring deformation character, are observed slightly to the blue at 1615 cm<sup>-1</sup> in the IRMPD spectra.

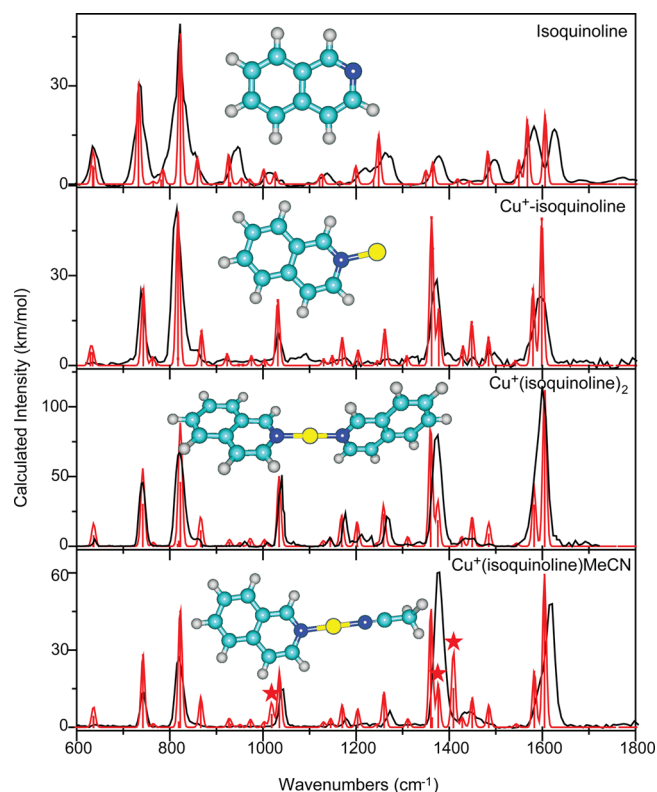


**Figure 3.** Experimental IRMPD spectra (black) of complexes of Cu<sup>+</sup> and isoquinoline complexes between 600 and 1800 cm<sup>-1</sup> compared with computed spectra (red). Stars in the lower panel indicate vibrational bands due to the acetonitrile ligand. The units of km mol<sup>-1</sup> refer to the stick spectra only.

**Table 4. Comparison of Observed and Computed IR Absorption Bands of Cu<sup>+</sup>(isoquinoline) (MeCN)**

expt freq <sup>a</sup>	calc freq <sup>a</sup>	dev <sup>b</sup>	int <sup>c,d</sup>	description
741	742	-1	28	CH oop bend
821	822	-1	45	CH oop bend
	867		12	CH oop bend/oop ring deform
1041	1035	6	21	CNC-Cu stretch/CC stretch/CH ip bend/ip ring deform
	1177		7	CH ip bend/ip ring deform/CC & CNC-Cu stretch
	1203		7	CH ip bend/ip ring deform/CC & CNC stretch
1273	1260	13	14	CC stretch/CH ip bend/ip ring deform
1374	1360	14	44	CC stretch/CH ip bend/ip ring deform/CNC stretch
	1376		17	CH ip bend/ip ring deform/CC & CNC stretch/
	1409		15	CH <sub>3</sub> scissoring
	1409		15	CH <sub>3</sub> scissoring
1440	1449	-9	11	CH ip bend/ip ring deform/CC stretch/CNC-Cu stretch
1496	1485	11	8	CH ip bend/ip ring deform/CC stretch/CNC stretch
	1583		22	CC stretch/CNC-Cu stretch/CH ip bend/ip ring deform
1615	1604	11	59	CC stretch/CH ip bend/ip ring deform/CNC-Cu stretch

RMS deviation 9.3

<sup>a</sup>In cm<sup>-1</sup>. Calculated frequencies scaled by 0.965. <sup>b</sup>exp - calc. <sup>c</sup>In km/mol. <sup>d</sup>Only bands with intensities >5 km/mol are listed.

**3.2.3. IR Spectra of Cu<sup>+</sup>/Acridine Complexes.** The IRMPD spectra of complexes of Cu<sup>+</sup> and acridine are compared with their computed spectra in Figure 4. Again, we find generally good agreement between computed and observed spectra and we will discuss the main features based on the Cu<sup>+</sup>(acridine) (MeCN) data (see Table 5).

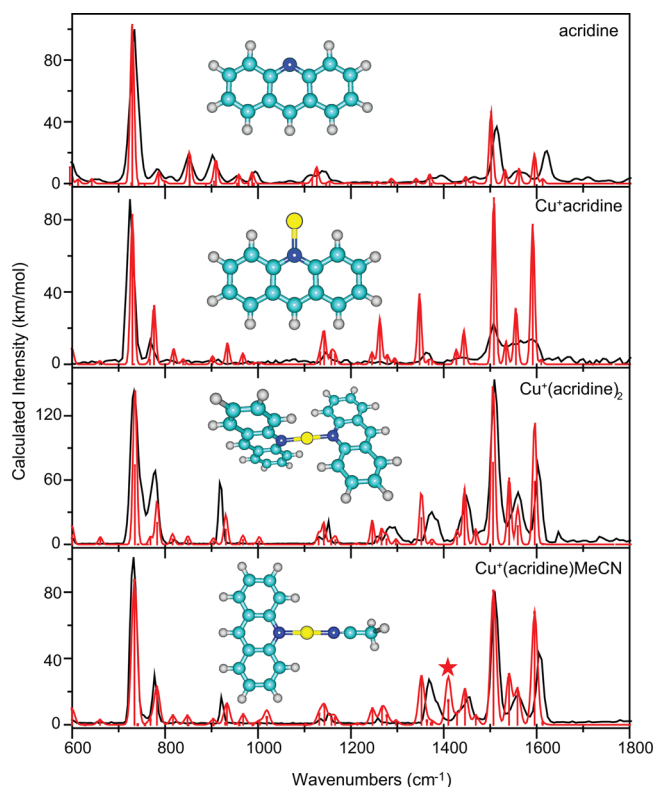


**Figure 4.** Experimental IRMPD spectra of Cu<sup>+</sup>/acridine complexes between 600 and 1800 cm<sup>-1</sup> (black) compared to the computed spectra (red). Stars in the lower panel indicate vibrational bands due to the acetonitrile ligand. The units of km mol<sup>-1</sup> refer to the stick spectra only.

The bands computed at 734 and 782 cm<sup>-1</sup> are due to CH oop bending and oop ring deformation and are observed in the experimental spectrum with a minimal red shift. The weaker band computed at 933 cm<sup>-1</sup> exhibits a larger red shift at 921 cm<sup>-1</sup>. Two weak bands computed at 1247 and 1267 cm<sup>-1</sup> represent modes involving CNC–Cu<sup>+</sup> symmetric stretching, CC stretching, and CH ip bending mixed with ip ring deformation and are observed as a weak feature at 1258 cm<sup>-1</sup>. Again, significant deviation between theory and experiment occurs around 1400 cm<sup>-1</sup>: computed bands in this range are due to a mode with mixed in-plane character at 1352 cm<sup>-1</sup> and bands due to the acetonitrile degenerate CH<sub>3</sub> bending mode at 1410 cm<sup>-1</sup> (indicated with a red star). The experimental spectrum exhibits a somewhat broader band in between those predicted bands, near 1368 cm<sup>-1</sup>. Two computed bands at 1446 and 1469 cm<sup>-1</sup> having mixed CC stretching, CH ip bending, ip ring deformation, and CNC symmetric stretching character are observed as a single feature centered at 1453 cm<sup>-1</sup>. A strong band with mixed in-plane character observed at 1510 cm<sup>-1</sup> is closely reproduced in the calculation at 1507 cm<sup>-1</sup>. Two computed bands around 1541 and 1559 cm<sup>-1</sup> are unresolved in the experiment at about 1558 cm<sup>-1</sup>. Finally, a strong band predicted at 1596 cm<sup>-1</sup>

**Table 5.** Comparison of Observed and Computed IR Absorption Bands of Cu<sup>+</sup>(acridine) (MeCN)

expt freq <sup>a</sup>	calc freq <sup>a</sup>	dev <sup>b</sup>	int <sup>c,d</sup>	description
732	734	-2	87	CH oop bend
777	782	-5	23	CH oop bend/oop ring deform
	816		5	CH op bend/oop ring deform/CC&CNC stretch
	848		5	CH op bend/oop ring deform/CC&CNC stretch
921	933	-12	12	CH oop bend/oop ring deform
	968		6	CH oop bend/oop ring deform
	1132		6	CH ip bend/ip ring deform/CNC-Cu&CC stretch
1151	1143	8	11	CH ip bend/ip ring deform/CNC-Cu&CC stretch
	1247		10	CNC-Cu&CC stretch/CH ip bend/ip ring deform
1258	1267	-9	10	CH ip bend/ip ring deform/CNC-Cu&CC stretch
	1277		5	CNC &CC stretch/CH ip bend/ip ring deform
1368	1352	16	29	CC stretch/CH ip bend/ip ring deform/CNC stretch
	1410		15	CH <sub>3</sub> bending
	1410		14	CH <sub>3</sub> bending
	1428		7	CC stretch/CH ip bend/ip ring deform/CNC stretch
1453	1446	7	21	CC stretch/CH ip bend/ip ring deform/CNC stretch
	1469		5	CC stretch/CH ip bend/ip ring deform/CNC stretch
1510	1507	3	81	CNC&CC stretch/CH ip bend/ip ring deform
	1541		30	CC stretch/CH ip bend/ip ring deform/CNC-Cu stretch
1558	1559	-1	22	CC stretch/CH ip bend/ip ring deform/CNC stretch
1604	1596	8	68	CC stretch/CH ip bend/ip ring deform/CNC stretch
				RMS deviation 8.3

<sup>a</sup>In cm<sup>-1</sup>. Calculated frequencies scaled by 0.965. <sup>b</sup>exp – calc. <sup>c</sup>In km/mol. <sup>d</sup>Only bands with intensities >5 km/mol are listed.

corresponding to a mode with mixed in-plane vibrational character is detected slightly to the blue at 1604 cm<sup>-1</sup>, as was also the case for the quinoline and isoquinoline complexes. Note that these bands appear to be better reproduced in the spectra of the Cu<sup>+</sup>(PANH) and Cu<sup>+</sup>(PANH)<sub>2</sub> complexes.

#### 4. DISCUSSION

Overall good agreement is found between experimental and computed band positions with deviations typically below 10 cm<sup>-1</sup>. This provides confidence that the structures in which the Cu<sup>+</sup> ion forms a  $\sigma$ -bond with the N atom of the PANH are indeed the correct ones, as also established by Rodgers and co-workers;<sup>61,62</sup>  $\pi$ -bonded Cu<sup>+</sup>PANH structures appear not to correspond to minima on the PES. In general, a single frequency scaling factor provides an adequate prediction of the spectra of the various Cu<sup>+</sup>PANH species over the 600–1800 cm<sup>-1</sup> spectral range. Some recurring deviations between experiment and theory are, however, also noticeable. Across the set of molecules studied here, we observe a 15 to 20 cm<sup>-1</sup> blue shift of the experimental band around 1360 cm<sup>-1</sup> as compared to its theoretical counterpart. This discrepancy is seen in the Cu<sup>+</sup>(PANH) (MeCN) as well as in the

$\text{Cu}^+(\text{PANH})_2$  complexes and therefore appears not to be related to MeCN. The associated normal modes have primarily PANH CC-stretching character, where the vibration involves in all cases mostly the bridgehead C atoms (see Figure S1 in the Supporting Information for a pictorial representation of these normal modes). The NBO calculations suggest low occupancies in the  $\pi$ -bonds connecting these bridgehead C atoms of around 1.5, compared to a typical value of about 1.7 for the other  $\pi$ -bonds in the PANH ligands. If this mode is ignored, the rms deviation between experimental and theoretical band positions reduces to about  $7\text{ cm}^{-1}$ , close to the bandwidth of the laser radiation and clearly less than the observed bandwidths in the spectra.

In all  $\text{Cu}^+(\text{PANH})$  (MeCN) spectra, bands predicted to be due to the MeCN ligand, indicated with stars in Figures 2–4, are not observed in the experimental spectra. The degenerate bending vibration of the methyl group computed to fall near  $1400\text{ cm}^{-1}$  is the most prominent example. We speculate that this may be due to incomplete energy randomization upon excitation of vibrations in the small MeCN ligand. Redistribution of vibrational energy (IVR) into the large bath of states of the PANH may be impeded by channeling of the vibrational energy through the heavy Cu atom. This effect has been suggested and described in more detail by Schröder and co-workers.<sup>74</sup> Inefficient IVR is expected to induce slow multiple photon absorption rates, so that the ion may not reach the dissociation threshold within the duration of the FEL pulse.

The intensities and positions of absorption bands are affected when  $\text{Cu}^+$  forms a complex with the PANHs. From the computed spectra in Figures 2–4 it is clear that in comparison with the neutral PANH spectra, all  $\text{Cu}^+$ -complexed PANHs exhibit a gain in intensity for the in-plane modes between  $1200$  and  $1800\text{ cm}^{-1}$  relative to that for the out-of-plane modes in the  $700$ – $900\text{ cm}^{-1}$  range. We suggest that this effect is caused by electron density transfer from the ligand to the metal ion, effectively giving the ligand partial cationic character, as indicated by the computed partial charges in Table 1. CC-stretching and CH in-plane bending modes are known to be strongly enhanced in ionized PAHs as compared to neutral PAHs.<sup>14,53,75–78</sup>

While the band positions for the  $\text{Cu}^+/\text{PANH}$  systems are generally well predicted, there appears to be a systematic offset between computed and experimental band positions for the neutral PANH species (spectra taken from NIST WebBook). It appears that the scaling factor used is too small for bands roughly above  $1000\text{ cm}^{-1}$  and that two different scaling factors may better reproduce the experimental data. On the other hand, we note that the value used is very close to recommended values for this combination of functional and basis set<sup>67,68</sup> and that this single scaling factor is generally adequate for the spectra of  $\text{Cu}^+/\text{PANH}$  systems.

Before we compare experimental spectra of the neutral PANHs with their copper cationized complexes below, we assess a possible redshift of vibrational bands induced by the IRMPD method applied to obtain the spectra of the complexes. For spectra of radical cation PAH species, we have in a previous paper<sup>73</sup> compared IRMPD band positions with band positions from matrix isolation spectroscopy (which themselves may have a small unknown shift compared with “true” but unavailable gas-phase transmission spectra<sup>79</sup>) and found red shifts typically in the range from  $5$  to  $40\text{ cm}^{-1}$ . However, the dissociation thresholds for the expulsion of one or more  $\text{C}_2\text{H}_n$  units, upon

which these spectra are based, are considerably higher ( $>400\text{ kJ mol}^{-1}$ )<sup>80–82</sup> than the threshold for the expulsion of a ligand from the  $\text{Cu}^+/\text{PANH}$  systems studied here ( $200$ – $300\text{ kJ mol}^{-1}$ ); moreover, the  $\text{Cu}^+/\text{PANH}$  systems likely dissociate via loose transition states, which is not at all the case for PAH breakdown,<sup>80,81,83,84</sup> further increasing the difference in endoergicity, which ought to result in a much reduced IRMPD redshift<sup>82,85</sup> for the  $\text{Cu}^+/\text{PANH}$  systems as compared to the PAH radical cations. If dissociation is facile, band shifts between IRMPD spectra and low-temperature tagging spectra may even become negligible.<sup>86</sup> We have therefore included the  $\text{Cu}^+(\text{PANH})$  (MeCN) complexes in our study, as the MeCN has a particularly low binding energy (Table 2). The fact that all three types of complexes— $\text{Cu}^+\text{PANH}$ ,  $\text{Cu}^+(\text{PANH})_2$ , and  $\text{Cu}^+(\text{PANH})$  (MeCN)—are well modeled with one and the same scaling factor suggests that band shifts due to IRMPD are minimal.

Across the three PANH molecules studied here, band positions of specific vibrational modes of the PANHs are consistently affected upon binding to  $\text{Cu}^+$ . The bands around  $1600\text{ cm}^{-1}$  are of special interest from an astrophysical standpoint. In Figure 5, we show the summed spectra of the

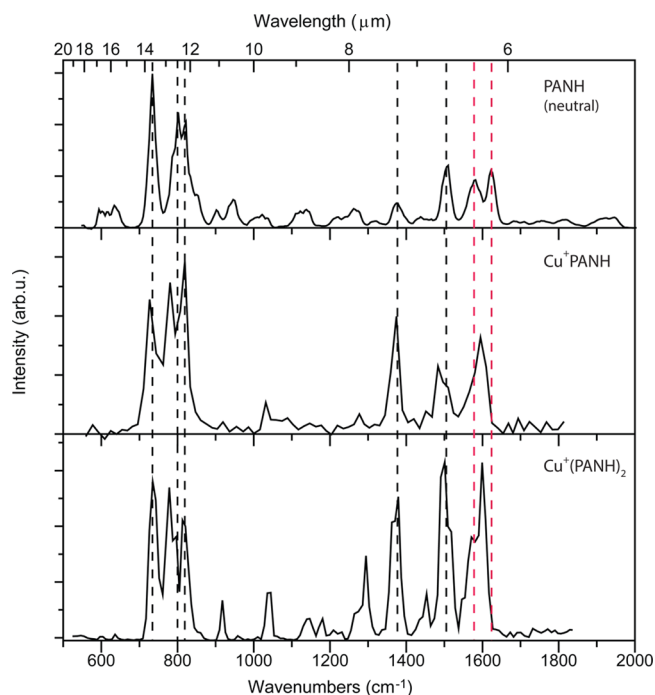


**Figure 5.** Sum of experimental IR spectra of quinoline, isoquinoline, and acridine as neutral uncomplexed molecules (top), as  $\text{Cu}^+(\text{PANH})_1$  complexes (middle), and as  $\text{Cu}^+(\text{PANH})_2$  complexes (bottom). The dashed lines indicate the positions of the most prominent bands in the neutral PANH sample; the red dashed lines fall closest to the interstellar  $6.2\text{ }\mu\text{m}$  feature.

three neutral PANHs, the three  $\text{Cu}^+(\text{PANH})_1$  complexes and the three  $\text{Cu}^+(\text{PANH})_2$  complexes, to illustrate the effect of  $\text{Cu}^+$  on the band positions (see also Table 6 and Supporting Tables S10–S12). Although the effect is modest, the absorption bands at  $1583$  and  $1622\text{ cm}^{-1}$  in the spectrum of the neutral PANHs (marked with red dashed lines) merge into a single absorption band at  $1595\text{ cm}^{-1}$  for  $\text{Cu}^+(\text{PANH})_1$  and at  $1599\text{ cm}^{-1}$  for  $\text{Cu}^+(\text{PANH})_2$  complexes. Bands in the vicinity, particularly near  $1400$  and  $1500\text{ cm}^{-1}$  (black dashed lines)

**Table 6.** Comparison of Observed IR Absorption Band Frequencies of the Summed Cu<sup>+</sup>/PANH Spectra Shown in Figure 5

neutral PANH		Cu <sup>+</sup> (PANH) <sub>1</sub>		Cu <sup>+</sup> (PANH) <sub>2</sub>	
cm <sup>-1</sup>	μm	cm <sup>-1</sup>	μm	cm <sup>-1</sup>	μm
734	13.6	727	13.8	735	13.6
802	12.5	780	12.8	778	12.9
822	12.2	819	12.2	817	12.2
1376	7.27	1374	7.28	1379	7.25
1509	6.63	1490	6.71	1496	6.68
1582	6.32				
1622	6.17	1595	6.27	1599	6.25

appear to undergo a smaller or no red shift, suggesting once more that the effect is largely due to Cu<sup>+</sup> coordination and not due to a possible IRMPD-induced redshift. Hence, we conclude that the bands near 1600 cm<sup>-1</sup>, which have the strongest CNC stretch character, are red-shifted by up to 20 cm<sup>-1</sup> upon Cu<sup>+</sup>-coordination. The band in the uncomplexed PANH species is closer to the interstellar 6.2 μm (1612 cm<sup>-1</sup>) band and Cu<sup>+</sup> complexation causes a modest shift away from that position. We note that despite the generally good agreement between experimental and theoretical spectra for the Cu<sup>+</sup>/PANH complexes (Figures 2–4), this sensitive red shift is not clearly reproduced in the B3LYP computed spectra. The bands associated with the CH-oop bending motion located around 802 cm<sup>-1</sup> for the neutral PANHs are red-shifted toward 12.7 μm (787 cm<sup>-1</sup>).

## 5. CONCLUSIONS

Infrared spectra have been recorded for a series of small gaseous Cu<sup>+</sup>/PANH complexes. The experimental spectra are compared with calculated spectra, which suggest that the Cu<sup>+</sup> ion coordinates to the lone-pair on the N atom, forming planar σ-bound complexes. This is in contrast with structures found for regular PAHs complexed with Ag<sup>+</sup> that were established to be π-bound.<sup>60</sup> On the other hand, this binding mode is analogous to that known for other metal ions binding to N-containing heterocycles.<sup>47,61,62,69</sup>

The DFT computed scaled harmonic frequencies generally reproduce the experimental Cu<sup>+</sup>/PANH spectra very well in the investigated 600–1800 cm<sup>-1</sup> range, with deviations typically below 10 cm<sup>-1</sup>, except for a specific CC stretch vibration near 1360 cm<sup>-1</sup>. Moreover, comparing spectra for the neutral PANH with those for the Cu<sup>+</sup> complexes in the 6 μm region, the subtle red shift (about 20 cm<sup>-1</sup>) observed for the dominant CNC-stretching band upon Cu<sup>+</sup> binding to the PANH molecules is not clearly reproduced by the current level of theory. Hence, whereas nitrogen inclusion into the PAH network induces a blue shift of the aromatic CC stretching modes toward the 6.2 μm astronomical emission band, σ-binding of a Cu<sup>+</sup> ion appears to induce a small but consistent red shift.

Intensities in the 1000–1600 cm<sup>-1</sup> frequency range are significantly enhanced with respect to bands in the 600–1000 cm<sup>-1</sup> region. This suggests significant charge transfer from the PANH ligands to the Cu cation, as confirmed by the NPA calculations, giving the ligands more cationic character. As a result, the spectra resemble more those of the cationic PANH species.

## ■ ASSOCIATED CONTENT

### 📄 Supporting Information

The Supporting Information is available free of charge on the ACS Publications website at DOI: 10.1021/acs.jpca.6b05060.

Normal mode visualization for CC-stretch mode near 1370 cm<sup>-1</sup> involving mainly the bridgehead C atoms; listings of experimental and theoretical frequencies for the Cu<sup>+</sup>(PANH) and Cu<sup>+</sup>(PANH)<sub>2</sub> complexes; tables with comparisons of experimental frequencies for each of the series of Cu<sup>+</sup>/PANH complexes studied (PDF)

## ■ AUTHOR INFORMATION

### Corresponding Author

\*Phone: (+31) 24 3653950. E-mail: joso@science.ru.nl

### Notes

The authors declare no competing financial interest.

## ■ ACKNOWLEDGMENTS

We gratefully acknowledge the FELIX staff for the skillful technical support and Mr. Musleh Munshi for additional DFT calculations. This work is sponsored by the Nederlandse Organisatie voor Wetenschappelijk Onderzoek (NWO) Physical and Chemical Sciences (EW/CW) as part of the Dutch Astrochemistry Network (DAN), under VICI Grant No. 724.011.002 (J.O.) and under VENI grant No. 722.013.014 (J.B.). It was further supported by NWO Physical Sciences (E.W.) for the use of the supercomputer facilities at SurfSara. J.O. thanks the Stichting Physica. This work is part of the research program of FOM, which is financially supported by NWO.

## ■ REFERENCES

- Allamandola, L. J.; Tielens, A. G. G. M.; Barker, J. R. Interstellar polycyclic aromatic hydrocarbons: the infrared emission bands, the excitation/emission mechanism, and the astrophysical implications. *Astrophys. J., Suppl. Ser.* **1989**, *71*, 733–775.
- Tielens, A. G. G. M. Interstellar Polycyclic Aromatic Hydrocarbon Molecules. *Annu. Rev. Astron. Astrophys.* **2008**, *46*, 289–337.
- Leger, A.; Puget, J. L. Identification of the ‘unidentified’ IR emission features of interstellar dust? *Astron. Astrophys.* **1984**, *137*, L5–L8.
- Allamandola, L. J.; Tielens, A. G. G. M.; Barker, J. R. Polycyclic aromatic hydrocarbons and the unidentified infrared emission bands: auto exhaust along the milky way! *Astrophys. J.* **1985**, *290*, L25–L28.
- Peeters, E. Astronomical observations of the PAH emission bands. *PAHs and the Universe: A Symposium to Celebrate the 25th Anniversary of the PAH Hypothesis*, Toulouse, France, 2011.
- Peeters, E.; Hony, S.; Van Kerckhoven, C.; Tielens, A. G. G. M.; Allamandola, L. J.; Hudgins, D. M.; Bauschlicher, C. W. The rich 6 to 9 μm spectrum of interstellar PAHs. *Astron. Astrophys.* **2002**, *390*, 1089–1113.
- Hudgins, D. M.; Allamandola, L. J. The spacing of the interstellar 6.2 and 7.7 micron emission features as an indicator of polycyclic aromatic hydrocarbon size. *Astrophys. J.* **1999**, *513*, L69–L73.
- Hudgins, D. M.; Allamandola, L. J. Infrared Spectroscopy of Matrix-Isolated Polycyclic Aromatic Hydrocarbon Cations. 2. The Members of the Thermodynamically Most Favorable Series through Coronene. *J. Phys. Chem.* **1995**, *99*, 3033–3046.
- Hudgins, D. M.; Bauschlicher, C. W., Jr.; Allamandola, L. J. Variations in the peak position of the 6.2 μm interstellar emission feature: a tracer of N in the interstellar polycyclic aromatic hydrocarbon population. *Astrophys. J.* **2005**, *632*, 316–332.
- Bauschlicher, C. W., Jr. The Infrared Spectra of C<sub>96</sub>H<sub>24</sub><sup>+</sup>, C<sub>96</sub>H<sub>24</sub><sup>+</sup>, and C<sub>96</sub>H<sub>25</sub><sup>+</sup>. *Astrophys. J.* **2002**, *564*, 782–786.

- (11) Hudgins, D. M.; Allamandola, L. J. Polycyclic Aromatic Hydrocarbons and Infrared Astrophysics: The State of the PAH Model and a Possible Tracer of Nitrogen in Carbon-rich Dust. In *Astrophysics of Dust*; Witt, A. N., Clayton, G. C., Draine, B. T., Eds.; Astronomical Society of the Pacific: San Francisco, CA, 2004; Vol. 309, pp 665–688.
- (12) Mattioda, A. L.; Hudgins, D. M.; Bauschlicher, C. W., Jr; Rosi, M.; Allamandola, L. J. Infrared Spectroscopy of Matrix-Isolated Polycyclic Aromatic Compounds and Their Ions. 6. Polycyclic Aromatic Nitrogen Heterocycles. *J. Phys. Chem. A* **2003**, *107*, 1486–1498.
- (13) Mattioda, A. L.; Hudgins, D. M.; Bauschlicher, C. W.; Allamandola, L. J. Infrared spectroscopy of matrix-isolated polycyclic aromatic compounds and their ions. 7. Phenazine, a dual substituted polycyclic aromatic nitrogen heterocycle. *Adv. Space Res.* **2005**, *36*, 156–165.
- (14) Alvaro Galué, H.; Piralí, O.; Oomens, J. Gas-phase infrared spectra of cationized nitrogen-substituted polycyclic aromatic hydrocarbons. *Astron. Astrophys.* **2010**, *517*, A15.
- (15) Gratton, R.; Sneden, C.; Carretta, E. Abundance Variations within Globular Clusters. *Annu. Rev. Astron. Astrophys.* **2004**, *42*, 385–440.
- (16) Kraft, R. P. Abundance Differences Among Globular-Cluster Giants: Primordial Versus Evolutionary Scenarios. *Publ. Astron. Soc. Pac.* **1994**, *106*, 553–565.
- (17) Smith, G. H. The chemical inhomogeneity of globular clusters. *Publ. Astron. Soc. Pac.* **1987**, *99*, 67–90.
- (18) Sneden, C. In *Galaxy Evolution: Connecting the Distant Universe with the Local Fossil Record*. *Astrophys. Space Sci.* **1999**, *265*, 145–152.
- (19) Sneden, C. In *The Galactic Halo: From Globular Clusters to the Field Stars*; Proceedings of the 35th Liege International Astrophysical Colloquium; L’Institut: Paris, 2000.
- (20) Morton, D. C.; Drake, J. F.; Jenkins, E. B.; Rogerson, J. B.; Spitzer, L.; York, D. G. Spectrophotometric results from the Copernicus satellite. II. Composition of interstellar clouds. *Astrophys. J.* **1973**, *181*, L103–L109.
- (21) Morton, D. C. Interstellar absorption lines in the spectrum of zeta ophiuchi. *Astrophys. J.* **1975**, *197*, 85–115.
- (22) Jenkins, E. B. In *Interstellar Processes*; Hollenbach, D. J., Thronson, H. A., Jr., Eds.; Springer: Dordrecht, The Netherlands, 1987; p 533.
- (23) Seab, C. G. Grain destruction, formation, and evolution. In *Interstellar Processes*; Astrophysics and Space Science Library; Springer: Dordrecht, The Netherlands, 1987; Vol. 134, p 490, DOI: 10.1007/978-94-009-3861-8\_18
- (24) Falgarone, E.; Puget, J. L.; Perault, M. The small-scale density and velocity structure of quiescent molecular clouds. *Astron. Astrophys.* **1992**, *257*, 715–730.
- (25) Falgarone, E.; Puget, J. L. The intermittency of turbulence in interstellar clouds: implications for the gas kinetic temperature and decoupling of heavy particles from the gas motions. *Astron. Astrophys.* **1995**, *293*, 840–852.
- (26) Klotz, A.; Marty, P.; Boissel, P.; Serra, G.; Chaudret, B.; Daudey, J. P. Contribution of metal-bonded polycyclic aromatic hydrocarbons to the interstellar depletion. *Astron. Astrophys.* **1995**, *304*, 520–530.
- (27) Dunbar, R. C.; Petrie, S. Interstellar and Circumstellar Reaction Kinetics of Na<sup>+</sup>, Mg<sup>+</sup>, and Al<sup>+</sup> with Cyanopolynes and Polyynes. *Astrophys. J.* **2002**, *564*, 792–802.
- (28) Li, A.; Draine, B. T. Are Silicon Nanoparticles an Interstellar Dust Component? *Astrophys. J.* **2002**, *564*, 803–812.
- (29) Graedel, T. E.; Langer, W. D.; Frerking, M. A. The kinetic chemistry of dense interstellar clouds. *Astrophys. J., Suppl. Ser.* **1982**, *48*, 321–368.
- (30) Caselli, P.; Walmsley, C. M.; Terzieva, R.; Herbst, E. The Ionization Fraction in Dense Cloud Cores. *Astrophys. J.* **1998**, *499*, 234–249.
- (31) de Boisanger, C.; Helmich, F. P.; van Dishoeck, E. F. The ionization fraction in dense clouds. *Astron. Astrophys.* **1996**, *310*, 315–327.
- (32) Wooden, D. H.; Charnley, S. B.; Ehrenfreund, P. In *Comets II: Composition and Evolution of Interstellar Clouds*; Festou, M., Keller, H. U., Weaver, H. A., Eds.; University of Arizona Press: Tucson, AZ, 2005; pp 33–66.
- (33) Serra, G.; Chaudret, B.; Saillard, Y.; Le Beuze, A.; Rabaa, H.; Ristorcelli, I.; Klotz, A. Organometallic chemistry in the interstellar medium. I. Are organometallic reactions efficient processes in astrochemistry? *Astron. Astrophys.* **1992**, *260*, 489–493.
- (34) Ehrenfreund, P.; Irvine, W.; Becker, L.; Blank, J.; Brucato, J. R.; Colangeli, L.; Derenne, S.; Despois, D.; Dutrey, A.; Fraaije, H.; et al. Astrophysical and astrochemical insights into the origin of life. *Rep. Prog. Phys.* **2002**, *65*, 1427–1487.
- (35) Marty, P.; Serra, G.; Chaudret, B.; Ristorcelli, I. Iron-aromatics coordination in molecular clouds. *Astron. Astrophys.* **1994**, *282*, 916–923.
- (36) Klotz, A.; Marty, P.; Boissel, P.; de Caro, D.; Serra, G.; Mascetti, J.; de Parseval, P.; Derouault, J.; Daudey, J. P.; Chaudret, B. Possible contribution of organometallic species in the solar system ices. Reactivity and spectroscopy. *Planet. Space Sci.* **1996**, *44*, 957–965.
- (37) Ristorcelli, I.; Klotz, A. Organometallic catalysis for aromatic molecules formation in carbon rich envelopes. *Astron. Astrophys.* **1997**, *317*, 962–967.
- (38) Boissel, P. Organometallic chemistry and the interstellar medium: experimental evidence of coordination between metal cations and polycyclic hydrocarbons in the gas phase. *Astron. Astrophys.* **1994**, *285*, 33–36.
- (39) Hettich, R. L.; Jackson, T. C.; Stanko, E. M.; Freiser, B. S. Gas-Phase Photodissociation of Organometallic Ions: Bond Energy and Structure Determinations. *J. Am. Chem. Soc.* **1986**, *108*, 5086–5093.
- (40) Hettich, R. L.; Freiser, B. S. Spectroscopic and Thermodynamic Investigations of Transition-Metal Cluster Ions in the Gas Phase: Photodissociation of MFe<sup>+</sup>. *J. Am. Chem. Soc.* **1987**, *109*, 3537–3542.
- (41) Bauschlicher, C. W., Jr; Partridge, H.; Langhoff, S. R. Theoretical Study of Transition-Metal Ions Bound to Benzene. *J. Phys. Chem.* **1992**, *96*, 3273–3278.
- (42) Meyer, F.; Khan, F. A.; Armentrout, P. B. Thermochemistry of Transition Metal Benzene Complexes: Binding Energies of M(C<sub>6</sub>H<sub>6</sub>)<sub>x</sub><sup>+</sup> (x = 1, 2) for M = Ti to Cu. *J. Am. Chem. Soc.* **1995**, *117*, 9740–9748.
- (43) Marty, P.; de Parseval, P.; Klotz, A.; Serra, G.; Boissel, P. Organometallic reactions in the gas phase: measurements of the formation and dissociation rates of organometallic complexes. *Astron. Astrophys.* **1996**, *316*, 270–274.
- (44) Srzić, D.; Kazazić, S.; Kralj, B.; Klasinc, L.; Marsel, J.; Güsten, H.; McGlynn, S. P. The niobium and tantalum riddle: gas-phase monocation reactions with pyrene and pyrene-D10. *Int. J. Mass Spectrom.* **2003**, *230*, 135–140.
- (45) Szczepanski, J.; Wang, H. Y.; Vala, M.; Tielens, A. G. G. M.; Eyler, J. R.; Oomens, J. Infrared spectroscopy of gas-phase complexes of Fe<sup>+</sup> and polycyclic aromatic hydrocarbon molecules. *Astrophys. J.* **2006**, *646*, 666–680.
- (46) Simon, A.; Joblin, C.; Polfer, N. C.; Oomens, J. Infrared Spectroscopy of [XFeC<sub>2n</sub>H<sub>12</sub>]<sup>+</sup> (X = C<sub>3</sub>H<sub>3</sub>, C<sub>5</sub>(CH<sub>3</sub>)<sub>5</sub>) Complexes in the Gas Phase: Experimental and Computational Studies of Astrophysical Interest. *J. Phys. Chem. A* **2008**, *112*, 8551–8560.
- (47) Chakraborty, S.; Dopfer, O. Infrared spectrum of the Ag<sup>+</sup>-(pyridine)<sub>2</sub> ionic complex: probing interactions in artificial metal-mediated base pairing. *ChemPhysChem* **2011**, *12*, 1999–2008.
- (48) Pozniak, P. P.; Dunbar, R. C. Monomer and dimer complexes of coronene with atomic ions. *J. Am. Chem. Soc.* **1997**, *119*, 10439–10445.
- (49) Simon, A.; Joblin, C. Photodissociation of [Fe<sub>x</sub>(C<sub>24</sub>H<sub>12</sub>)<sub>y</sub>]<sup>+</sup> Complexes in the PIRENEA Setup: Iron-Polycyclic Aromatic Hydrocarbon Clusters as Candidates for Very Small Interstellar Grains. *J. Phys. Chem. A* **2009**, *113*, 4878–4888.
- (50) Simon, A.; Joblin, C. Thermochemistry and infrared spectroscopy of neutral and cationic iron-PAH complexes of astrophysical

interest: fundamental DFT studies. *J. Phys. Chem. A* **2007**, *111*, 9745–9755.

(51) Bauschlicher, C. W., Jr.; Ricca, A. The far-infrared emission from the Mg<sup>+</sup>-PAH species. *Astrophys. J.* **2009**, *698*, 275–280.

(52) Joalland, A.; Simon, A.; Marsden, C.; Joblin, C. Signature of SiPAH<sup>+</sup>  $\pi$ -Complexes in the interstellar medium. *Astron. Astrophys.* **2009**, *494*, 969–976.

(53) Allamandola, L. J.; Hudgins, D. M.; Sandford, S. A. Modeling the unidentified infrared emission with combinations of polycyclic aromatic hydrocarbons. *Astrophys. J.* **1999**, *511*, L115–L119.

(54) Simon, A.; Joblin, C. The computed IR spectra for a variety of FePAH<sup>+</sup> complexes: mid- and far-IR features. *Astrophys. J.* **2010**, *712*, 69–77.

(55) Joalland, A.; Rapacioli, M.; Simon, A.; Joblin, C.; Marsden, C.; Spiegelman, F. Molecular dynamics simulations of anharmonic infrared spectra of SiPAH<sup>+</sup>  $\pi$ -Complexes. *J. Phys. Chem. A* **2010**, *114*, 5846–5854.

(56) Simon, A.; Rapacioli, M.; Lanza, M.; Joalland, B.; Spiegelman, F. Molecular dynamics simulations on FePAH<sup>+</sup>  $\pi$ -complexes of astrophysical interest: anharmonic infrared spectroscopy. *Phys. Chem. Chem. Phys.* **2011**, *13*, 3359–3374.

(57) Roithová, J. Characterization of reaction intermediates by ion spectroscopy. *Chem. Soc. Rev.* **2012**, *41*, 547–559.

(58) Polfer, N. C.; Oomens, J. Reaction products in mass spectrometry elucidated with infrared spectroscopy. *Phys. Chem. Chem. Phys.* **2007**, *9*, 3804–3817.

(59) Eyler, J. R. Infrared multiple photon dissociation spectroscopy of ions in Penning traps. *Mass Spectrom. Rev.* **2009**, *28*, 448–467.

(60) Savoca, M.; Wende, T.; Jiang, L.; Langer, J.; Meijer, G.; Dopfer, O.; Asmis, K. R. Infrared Spectra and Structures of Silver–PAH Cation Complexes. *J. Phys. Chem. Lett.* **2011**, *2*, 2052–2056.

(61) Rannulu, N. S.; Rodgers, M. T. Solvation of copper ions by imidazole: Structures and sequential binding energies of Cu<sup>+</sup>(imidazole)<sub>x</sub>, x = 1–4. Competition between ion solvation and hydrogen bonding. *Phys. Chem. Chem. Phys.* **2005**, *7*, 1014–1025.

(62) Rannulu, N. S.; Rodgers, M. T. Noncovalent Interactions of Cu<sup>+</sup> with N-Donor Ligands (Pyridine, 4,4-Dipyridyl, 2,2-Dipyridyl, and 1,10-Phenanthroline): Collision-Induced Dissociation and Theoretical Studies. *J. Phys. Chem. A* **2007**, *111*, 3465–3479.

(63) Marshall, A. G.; Hendrickson, C. L.; Jackson, G. S. Fourier transform ion cyclotron resonance mass spectrometry: a primer. *Mass Spectrom. Rev.* **1998**, *17*, 1–35.

(64) Oepts, D.; Van Der Meer, A. F. G.; Van Amersfoort, P. W. The free-electron-laser user facility FELIX. *Infrared Phys. Technol.* **1995**, *36*, 297–308.

(65) Valle, J. J.; Eyler, J. R.; Oomens, J.; Moore, D. T.; van der Meer, A. F. G.; et al. Free electron laser-Fourier transform ion cyclotron resonance mass spectrometry facility for obtaining infrared multiphoton dissociation spectra of gaseous ions. *Rev. Sci. Instrum.* **2005**, *76*, 023103.

(66) Dunbar, R. C. Infrared radiative cooling of isolated polyatomic molecules. *J. Chem. Phys.* **1989**, *90*, 7369–7375.

(67) Johnson, R. D., III. In *NIST Standard Reference Database Number 101*; Johnson, R. D., III, Ed.; NIST: Gaithersburg, MD, 2015; Vol. 2016.

(68) Merrick, J. P.; Moran, D.; Radom, L. An evaluation of harmonic vibrational frequency scale factors. *J. Phys. Chem. A* **2007**, *111*, 11683–11700.

(69) Gao, J.; Berden, G.; Rodgers, M. T.; Oomens, J. Interaction of Cu<sup>+</sup> with cytosine and formation of i-motif-like C–M<sup>+</sup>–C complexes: alkali versus coinage metals. *Phys. Chem. Chem. Phys.* **2016**, *18*, 7269–7277.

(70) Lias, S. G. In *NIST Chemistry WebBook, NIST Standard Reference Database Number 69: Ionization Energy Evaluation*; Linstrom, P. J., Mallard, W. G., Eds.; National Institute of Standards and Technology: Gaithersburg, MD; retrieved January 22, 2016; Vol. 69.

(71) *NIST Chemistry Webbook, Standard Reference Database Number 69*; Linstrom, P. J.; Mallard, W. G., Eds.; National Institute of Standards and Technology: Gaithersburg MD, 2009; Vol. 69.

(72) Stein, S. E. In *NIST Standard Reference Database Number 69*; Linstrom, P. J., Mallard, W. G. E., Eds.; National Institute of Standards and Technology: Gaithersburg MD; retrieved August 20, 2015.

(73) Oomens, J.; Tielens, A. G. G. M.; Sartakov, B. G.; von Helden, G.; Meijer, G. Laboratory infrared spectroscopy of cationic polycyclic aromatic hydrocarbon molecules. *Astrophys. J.* **2003**, *591*, 968–985.

(74) Shaffer, C. J.; Révész, Á.; Schröder, D.; Severa, L.; Teplý, F.; Zins, E.-L.; Jasiková, L.; Roithová, J. Can Hindered Intramolecular Vibrational Energy Redistribution Lead to Non-Ergodic Behavior of Medium-Sized Ion Pairs? *Angew. Chem., Int. Ed.* **2012**, *51*, 10050–10053.

(75) Pauzat, F.; Talbi, D.; Miller, M. D.; DeFrees, D. J.; Ellinger, Y. Theoretical IR spectra of ionized naphthalene. *J. Phys. Chem.* **1992**, *96*, 7882–7886.

(76) Szczepanski, J.; Roser, D.; Personette, W.; Eyring, M.; Pellow, R.; Vala, M. Infrared spectrum of matrix-isolated naphthalene radical cation. *J. Phys. Chem.* **1992**, *96*, 7876–7881.

(77) Knorke, H.; Langer, J.; Oomens, J.; Dopfer, O. Infrared spectra of isolated protonated polycyclic aromatic hydrocarbon molecules. *Astrophys. J.* **2009**, *706*, L66–L70.

(78) DeFrees, D. J.; Miller, M. D. The effect of ionization on the infrared absorption spectra of PAHs: a preliminary report. *NASA, Ames Research Center, Interstellar Dust*; NASA: Santa Clara, CA, 1989.

(79) Joblin, C.; d'Hendecourt, L.; Léger, A.; Défourneau, D. Infrared spectroscopy of gas-phase PAH molecules. I. Role of the physical environment. *Astron. Astrophys.* **1994**, *281*, 923–936.

(80) Dyakov, Y. A.; Ni, C.-K.; Lin, S. H.; Lee, Y. T.; Mebel, A. M. Ab initio and RRKM study of photodissociation of azulene cation. *Phys. Chem. Chem. Phys.* **2006**, *8*, 1404–1415.

(81) Bouwman, J.; de Haas, J.; Oomens, J. Spectroscopic evidence for the formation of pentalene<sup>+</sup> in the dissociative ionization of naphthalene. *Chem. Commun.* **2016**, *52*, 2636–2638.

(82) Parneix, P.; Basire, M.; Calvo, F. Accurate Modeling of Infrared Multiple Photon Dissociation Spectra: The Dynamical Role of Anharmonicities. *J. Phys. Chem. A* **2013**, *117*, 3954–3959.

(83) West, B.; Sit, A.; Mohamed, S.; Joblin, C.; Blanchet, V.; Bodi, A.; Mayer, P. M. Dissociation of the Anthracene Radical Cation: A Comparative Look at iPEPICO and Collision-Induced Dissociation Mass Spectrometry Results. *J. Phys. Chem. A* **2014**, *118*, 9870–9878.

(84) Petrigiani, A.; Vala, M.; Eyler, J. R.; Tielens, A. G. G. M.; Berden, G.; Van der Meer, A. F. G.; Redlich, B.; Oomens, J. Breakdown products of gaseous polycyclic aromatic hydrocarbons investigated with infrared ion spectroscopy. *Astrophys. J.* **2016**, *826*, 33.

(85) Oomens, J.; Moore, D. T.; Meijer, G.; von Helden, G. Infrared multiple photon dynamics and spectroscopy of cationic PABA and its dehydroxylated fragment ion. *Phys. Chem. Chem. Phys.* **2004**, *6*, 710–718.

(86) Kamrath, M. Z.; Garand, E.; Jordan, P. A.; Leavitt, C. M.; Wolk, A. B.; van Stipdonk, M. J.; Miller, S. J.; Johnson, M. A. Vibrational Characterization of Simple Peptides Using Cryogenic Infrared Photodissociation of H<sub>2</sub>-Tagged, Mass-Selected Ions. *J. Am. Chem. Soc.* **2011**, *133*, 6440–6448.

## ■ NOTE ADDED AFTER ASAP PUBLICATION

This article was published ASAP on September 30, 2016. Figure 4 and Table 6 have been updated and the corrected version was reposted on October 3, 2016.